ACS APPLIED MATERIALS & INTERFACES

www.acsami.org

Research Article

Constructing High-Performance Yarn-Shaped Electrodes via Twisting-after-Coating Technique for Weavable Seawater Battery

Yihao Jian, Jun Ju, Lingwei Pei, Wenhu Gao, Duan Li, Wei Wang, Yan Qiao,* and Zhisong Lu*

Cite This: *ACS Appl. Mater. Interfaces* 2024, 16, 71038−71047

Read Online

ACCESS | Metrics & More | Article Recommendations | Supporting Information

ABSTRACT: Seawater batteries (SWBs) are green aqueous power sources with great potential in marine applications. So far, SWBs are mainly built on rigid substrates, which hinders their adaptability to marine textile applications. Herein, we constructed a rechargeable yarn-shaped SWB consisting of nickel hexacyanoferrate (Ni-HCF)-modified carbon yarn (positive electrode), glass fiber diaphragm, and polyimide (PI)-modified carbon yarn (negative electrode). To improve the performance of carbon yarn-based electrodes, a twisting-after-coating (TAC) technique was developed to replace the conventional twisting-before-coating (TBC) technique for immobilizing active materials. The TAC technique could fully utilize the internal spaces between adjacent fibers in carbon yarns and avoid the accumulation of active materials on the electrode surface. Taking the Ni-HCF-modified electrode as an example, its maximum specific capacity could reach 64.2 mAh/g, significantly higher than that (54.5 mAh/g) of the electrode prepared by the TBC technique. The improvement could be explained by embedding the active materials in the yarn and the close contact between the active materials and the carbon fibers caused by the twisting. The Ni-HCF-modified and PI-modified yarn electrodes prepared by the TAC technique were assembled to construct a yarn-shaped SWB that exhibits good rate performance, excellent flexibility, and high cycling stability. The yarn-shaped SWBs were further woven into a fishing net-like textile. After being soaked with seawater and electrically charged, the textile can successfully power a light panel composed of 10 light-emitting diodes, demonstrating the potential of yarn-shaped SWBs for power supply in marine.

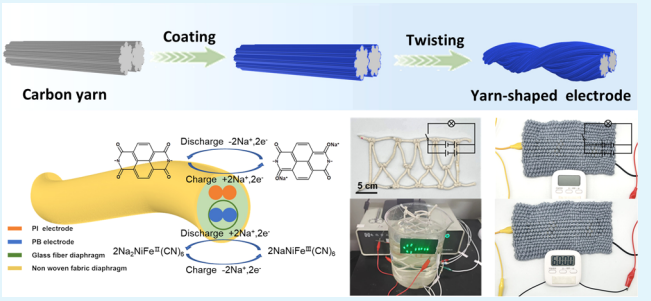

KEYWORDS: *yarn-shaped seawater battery, electrode modification, twisting-after-coating technique, flexibility, textile electronics*

INTRODUCTION

Seawater covers 71% of the Earth's surface, therefore being one of nature's most abundant water resources.[1] It is a multicomponent natural electrolyte comprising cations including Na^+, K^+, Ca^{2+}, and Mg^{2+}, as well as anions such as Cl^-, SO_4^{2-}, Br^-, HCO_3^-, and CO_3^{2-}. Its ionic conductivity can reach 50 $mS{\cdot}cm^{-1}$.[2] Seawater batteries (SWBs), which use natural seawater as an electrolyte, are green and environmentally friendly aqueous power devices.[3] The first generation of SWBs are primary batteries that use active metals as the anode materials.[4−6] Since the active metal anodes are continuously consumed during the operation, the batteries are unsuitable for long-term high-power applications. A new generation of rechargeable SWBs has been developed to store electrical energy using seawater as the cathode for sustainable power supply. These batteries utilize a Na super ion conductor (NASICON) membrane to separate the nonaqueous anolyte and the aqueous seawater catholyte.[7−10] The closed anode selectively harvests sodium ions from the open cathode during charging. Meanwhile, during discharging, the sodium ions are transferred back to the seawater side to supply the electricity.

Active metals such as Zn, Mg, and Al have been used as anode materials to construct rechargeable SWBs with a completely open structure to avoid the use of excessively active Na metal, organic electrolytes, and brittle ceramic membranes.[11−13] The cathode materials in these batteries could be carbon-based bifunctional electrocatalysts,[14] carbon felt−polypyrrole−silver chloride composite,[15] and Prussian blue analog.[16] Since Na^+ is the most abundant cation in seawater with a concentration of up to 0.47 M, the rapid progress of the aqueous sodium-ion battery inspires the development of rechargeable open-structure SWBs. In "rocking chair" sodium-ion batteries, the sodium ions are shuttled back and forth between the positive and negative electrodes by reverse intercalation and deintercalation during the charge/discharge cycles.[17] Therefore, the anode and cathode materials

Received: September 25, 2024
Revised: November 28, 2024
Accepted: November 29, 2024
Published: December 11, 2024

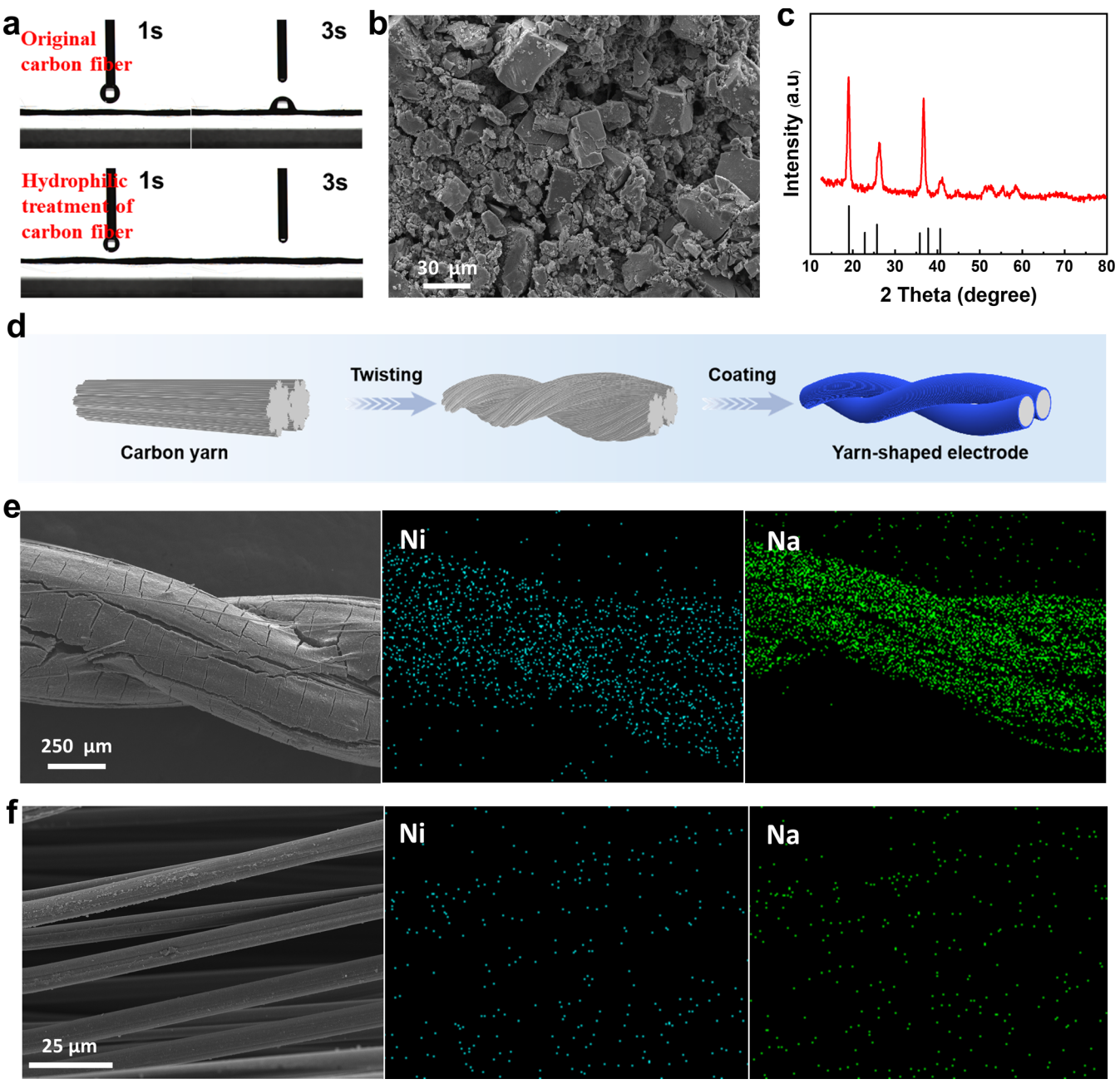

Figure 1. Yarn-shaped electrode prepared using conventional twisting-before-coating (TBC) method. (a) Hydrophilicity of carbon yarn before and after electrochemical treatment; SEM image (b) and XRD pattern (c) of Ni-HCF; (d) schematic diagram of the conventional TBC method for carbon yarn modification; (e) field emission SEM (FESEM) and energy dispersive spectroscopy (EDS) mapping images showing the surface of a yarn-shaped electrodes prepared with the TBC method; (f) FESEM and EDS mapping images showing the internal fibers in a yarn-shaped electrode prepared with the TBC method.

determine the overall performance of the sodium-ion battery. The lattice-expanded anatase TiO_2 has been prepared as an anode material to intercalate multiple cations (Na^+, Ca^{2+}, and Mg^{2+}) in seawater with high capacities for constructing membrane-less open-structure SWBs.[18] Polyimide (PI) has also been coupled with nickel hexacyanoferrate (Ni-HCF), a Prussian blue analog, as active materials to fabricate a rechargeable open-structure SWB.[19] Charging of the battery involves the association of Na^+ at the reduced carbonyl groups of PI and the deintercalation of Na^+ from the open lattice structure of Ni-HCF. During discharging, the sodium ions dissociated from the oxidized carbonyl groups of PI are embedded in the Ni-HCF cathode.

Textiles are used in marine applications such as sail suits, fishing nets, life jackets, mooring ropes, and diving suits. A power supply is also vital for illuminating, tracking, and communicating at night or in the deep sea. Various textile-based energy systems have been developed to power wearable electronic devices in the past few years.[20,21] Fiber- or yarn-shaped batteries have attracted the most interest due to their lightweight, flexibility, and weavability.[22] Fiber-shaped lithium-ion batteries, incorporating organic and gel electrolytes, have been successfully manufactured at an industrial scale, serving as

https://doi.org/10.1021/acsami.4c16439
ACS Appl. Mater. Interfaces 2024, 16, 71038−71047

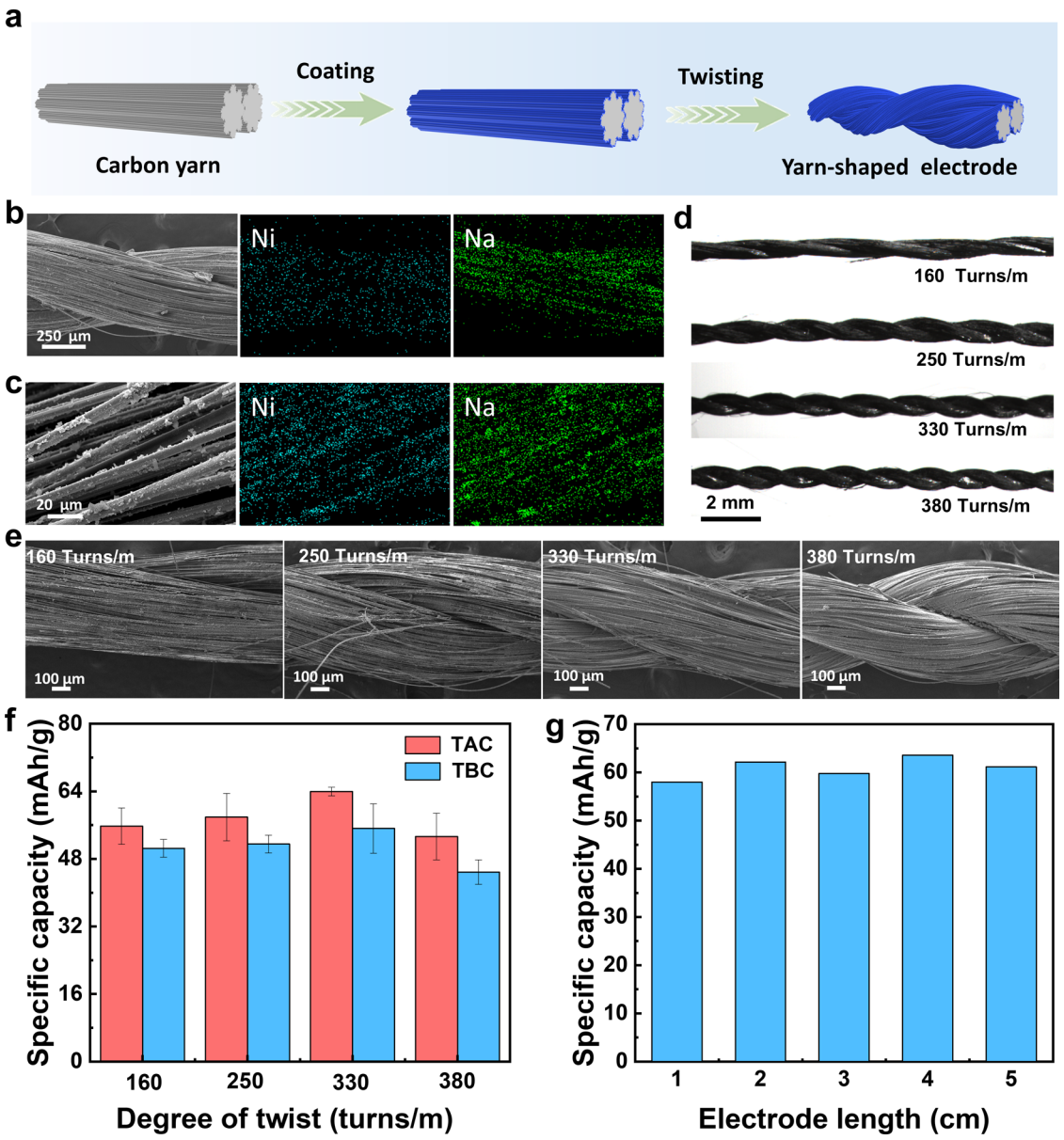

Figure 2. Yarn-shaped electrode prepared using TAC method. (a) Schematic diagram of the TAC method for carbon yarn modification; (b) FESEM and EDS mapping images showing the surface of a yarn-shaped electrode prepared with the TAC method; (c) FESEM and EDS mapping images showing the internal fibers in a yarn-shaped electrode prepared with the TAC method; micrographs (d) and SEM images (e) of yarn-shaped positive electrodes with different twist levels; (f) specific capacity of yarn-shaped positive electrodes with different twist levels prepared by TAC and TBC methods; (g) specific capacity of yarn-shaped positive electrodes with different lengths.

a viable power source for textile electronics.[23] In recent works, yarn-shaped sweat-activated batteries with segmental and core−sheath architectures have also been fabricated to power sensing devices for wearable exercise monitoring.[24,25] Although SWBs have demonstrated outstanding potential in marine applications, the current SWB designs are primarily based on rigid substrates, which limits their flexibility and compatibility with traditional textile technologies.[26,27] Therefore, there is a need to explore novel approaches to address these challenges and improve the adaptability of SWBs for marine textile applications.

Herein, we constructed a rechargeable high-performance yarn-shaped SWB consisting of nickel hexacyanoferrate (Ni-HCF)-modified carbon yarn (positive electrode), glass fiber diaphragm, and polyimide (PI)-modified carbon yarn (negative electrode). In contrast to the traditional electrode preparation method, in which active materials are coated on pretwisted carbon yarns (twisting-before-coating method, TBC), Ni-HCF or PI materials are modified on neatly aligned carbon fiber bundles, which are then twisted to form yarn electrodes (twisting-after-coating method, TAC), for weavable SWBs. The proposed TAC method can avoid the accumulation of active materials on the electrode surface and fully utilize the internal space between adjacent carbon fibers. Taking the Ni-HCF-modified electrode as an example, the TAC method can significantly increase the specific capacity. The capacity of the yarn electrode can be customized by adjusting the twist level of the yarn. The positive (Ni-HCF-modified) and negative (PI-modified) electrodes prepared by the TAC method were combined in a parallel structure to fabricate yarn-shaped SWBs with high capacity, excellent

https://doi.org/10.1021/acsami.4c16439
ACS Appl. Mater. Interfaces 2024, 16, 71038−71047

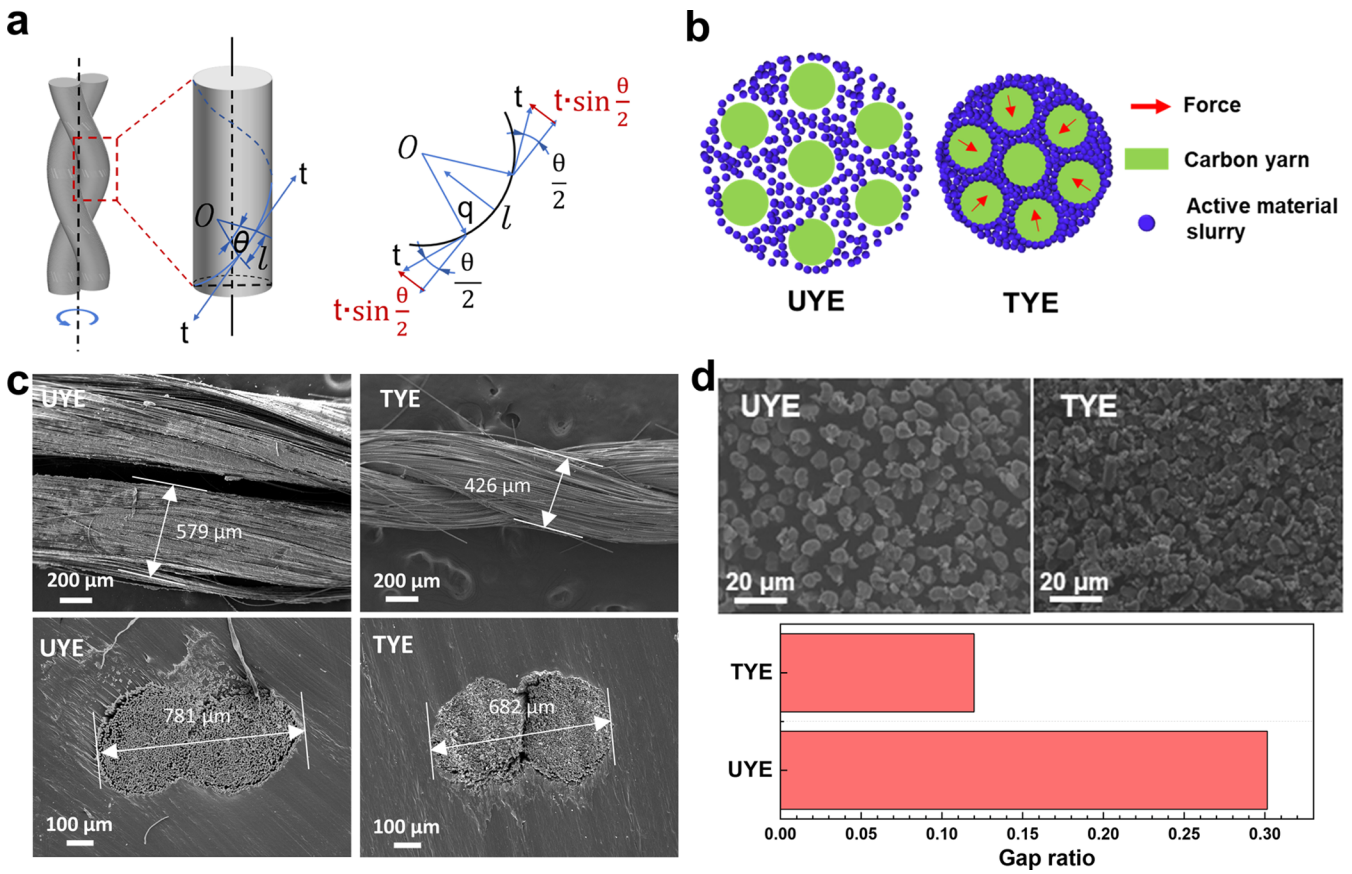

Figure 3. Possible mechanism for the high performance of the yarn electrode prepared via the TAC method. (a) Force analysis of an outermost fiber on the yarn surface; (b) schematic diagram showing an untwisted yarn electrode (UYE) and a twisted yarn electrode (TYE); (c) SEM images showing the width of a UYE and a TYE; (d) cross-sectional SEM images and gap ratios of a UYE and a TYE.

retention, and good flexibility. Their potential applications in seawater were also demonstrated as nets and fabrics.

RESULTS AND DISCUSSION

Carbon yarns have been widely used as current collectors to prepare flexible batteries and supercapacitors due to their excellent conductivity and chemical stability.[28] In the present study, active materials were coated on carbon yarns to fabricate one-dimensional electrodes for SWBs. Since enhancing wettability of yarns can facilitate the adhesion of active materials for high-performance electrodes,[29,30] the carbon yarn was treated with 2 M H_2SO_4 solution under cyclic voltammetry to introduce oxygen-containing hydrophilic groups on its surface. The hydrophilicity of the treated carbon yarns was significantly improved compared to the original carbon yarns (Figure 1a). Prussian blue and its analogs (PBAs) are transition metal hexacyanoferrites with metal−organic framework (MOF) structures. As a typical Ni-doped PBA, Ni-HCF exhibits extremely high lattice stability during intercalation and deintercalation of Na^+.[31,32] Therefore, we synthesized Ni-HCF powders using the coprecipitation method to serve as the active material of the positive electrode. As shown in Figure 1b, the as-prepared products are cubic-structured particles with a microscale size. The X-ray diffraction pattern exhibits eight peaks at 17.28, 24.51, 34.84, 38.86, 43.38, 49.89, 53.23, and 56.42°, corresponding to the (200), (220), (400), (420), (422), (440), (600), and (620) crystal planes of Ni-HCF, respectively (Figure 1c). The scanning electron microscopy (SEM) image and the XRD spectrum prove the successful synthesis of the MOF-structured Ni-HCF material.

As shown in Figure 1d, Ni-HCF-based yarn electrodes were fabricated using the conventional TBC technique. Carbon fibers are wound together to form a stable yarn structure. Then, the Ni-HCF-based slurry was pasted onto the carbon yarn to obtain the yarn-shaped positive electrode. Compared with the fiber bundles observed in the SEM image of the pretwisted carbon yarn (Figure S1), the yarn surface was coated by a thick film with many cracks. In addition, the EDS mapping images clearly show the uniform distribution of Ni and Na elements in the surface-coating layer (Figure 1e). To further check the distribution of active materials in the yarn, the as-prepared yarn electrode was disassembled to remove the surface-attached materials and unravel the carbon yarn. Unlike the dense accumulation of Ni-HCF on the yarn's surface, almost no active material was attached to the carbon fibers inside the yarn. The EDS images also show the absence of Ni and Na elements (Figure 1f). The results reveal that the active materials can be modified on the surface of the carbon yarn using the conventional TBC method but not in the internal space. The external buildup of active materials may increase electrode resistance and does not fully utilize carbon fibers inside the yarn.

To overcome the drawbacks of the conventional method, we propose a new method called the TAC technique for fabricating yarn-like electrodes. Carbon yarns purchased from the market were untwisted to obtain parallel aligned carbon fibers. Ni-HCF slurry was plated onto the untwisted carbon

https://doi.org/10.1021/acsami.4c16439
ACS Appl. Mater. Interfaces 2024, 16, 71038−71047

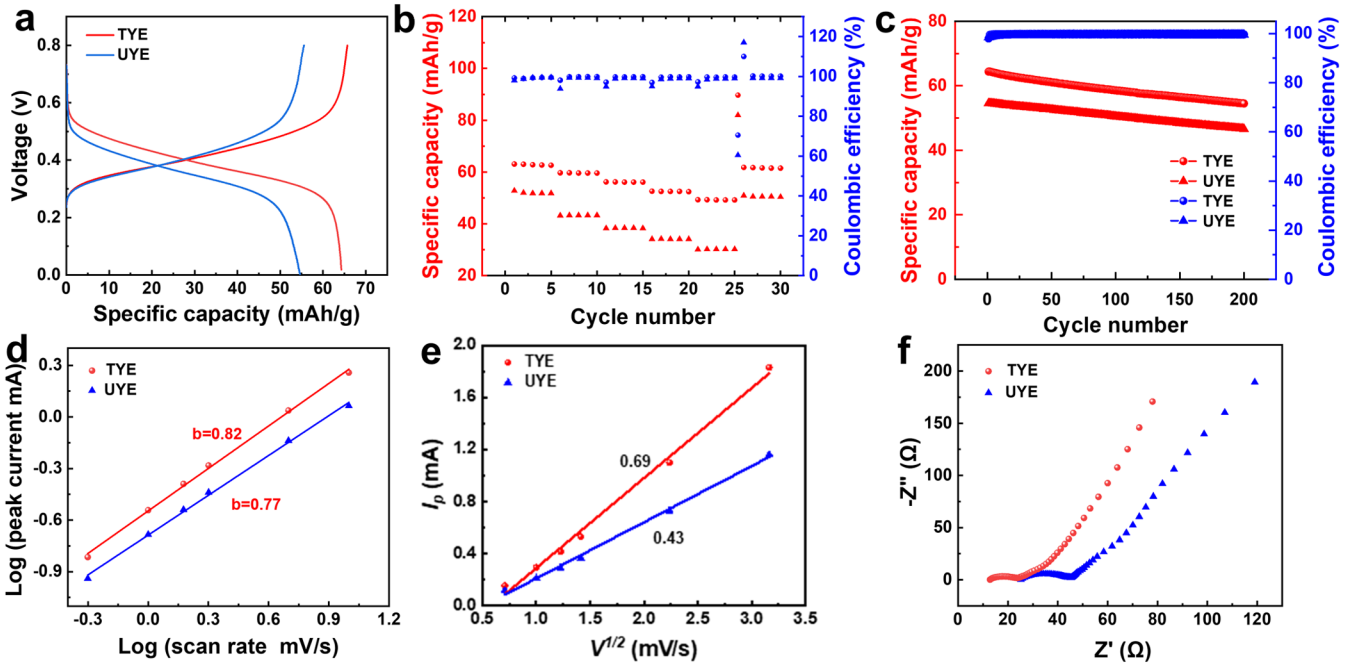

Figure 4. Electrochemical performance of UYE and TYE. (a) GCD curves of UYE and TYE under a current density of 1.0 A/g; (b) rate performance of UYE and TYE under different current densities (current densities from left to right are 1.0, 2.0, 3.0, 4.0, 5.0, and 1.0 A/g); (c) cycling performance of UYE and TYE at a current density of 1.0 A/g; (d) logarithmic relationship between the peak current I_p and the square root of the scanning rate $v^{1/2}$; (e) relationship between the peak current I_p and the square root of the scanning rate $v^{1/2}$; (f) Nyquist plots of full batteries prepared with UYE and TYE.

yarns to ensure sufficient coating of each fiber. Then, the modified carbon yarns were twisted to obtain yarn-shaped positive electrodes (Figure 2a). The twisted fibers and surface-attached particles can be seen from the SEM images. EDS images further demonstrate the uniform distribution of Ni-HCF on the electrode surface (Figure 2b). High-magnification SEM and EDS images show the attachment of Ni-HCF particles and the presence of characteristic elements (Ni and Na elements) on each internal fiber, respectively (Figure 2c). The above results indicate that using the TAC technique, the active materials can be embedded into the internal part of the carbon yarns to modify each carbon fiber uniformly. In addition, the surface accumulation of active materials observed in the TBC method can be avoided entirely, leading to the effective utilization of active materials and current collectors.

Twist is a critical process in yarn production that can hold the fibers together.[33] The level of twist could affect the size of the gaps between adjacent fibers in the yarn. In the present study, the yarn electrodes with twist levels of 160, 250, 330, and 380 turns/m were prepared to examine the effects of twist level on the electrode performance. The structure of the carbon yarn gradually changes from loose to dense as the twist level increases from 160 to 330 turns/m (Figure 2d). As the gaps between the neighboring fibers narrow, the active materials prepasted on the fibers extrude from the gaps to form extrudates on the yarn surface (Figure 2e). Electrochemical tests were conducted using a three-electrode system to measure the specific capacity of each Ni-HCF-modified electrode. Since there is no significant difference in the CV curves obtained in pure seawater and 0.5 mol/L NaCl solution (Figure S2), the NaCl solution was used to mimic seawater to investigate the electrochemical performance of the electrodes. It is worth noting that the ionic strength of the electrolyte may affect the intercalation and deintercalation of ions in the electrode materials, subsequently affecting the performance of the SWBs. Under the conditions mentioned above, the yarn-shaped electrodes prepared via the TAC method exhibit a superior specific capacity compared to those prepared through the conventional TBC method. As the twist level increases from 160 to 330 turns/m, the specific capacity of the yarn electrode prepared by the TAC method gradually enhances, reaching a maximum value of 64.0 ± 1.0 mAh/g at 330 turns/m (Figure 2f). An increase in twist to 380 turns/m results in a notable decline in specific capacity. As shown in Figure 2g, there is no significant variation in the specific capacity of the yarn electrodes with different lengths, indicating that the electrodes prepared via the TAC method possess excellent uniformity. The results suggest that the TAC approach may avoid the accumulation of active materials on the external surface and effectively utilize the internal gaps of the yarn to achieve a high specific capacity. Furthermore, the performance of the yarn-based electrode can be tuned by tailoring the twist level of the yarn after the coating process. Given that the highest specific capacity was obtained at a twist level of 330 turns/m, it was selected as the optimal twist level for preparing the yarn electrode via the TAC method in subsequent experiments.

During the twisting process, the outermost fibers parallel with the yarn axes gradually incline to form an angel, finally wrapping around the yarn. A force analysis was performed on a fiber located at the outermost part of the yarn to explore the mechanism for the twisting-caused enhancement of the specific capacity. As shown in Figure 3a, a segment of the outer fiber with the length of l twists around the yarn, forming a central angle of θ. The twisting causes the stretching of the fiber along its axial direction to generate the tension t, which further results in the compression force q toward the core. The

https://doi.org/10.1021/acsami.4c16439
ACS Appl. Mater. Interfaces 2024, 16, 71038−71047

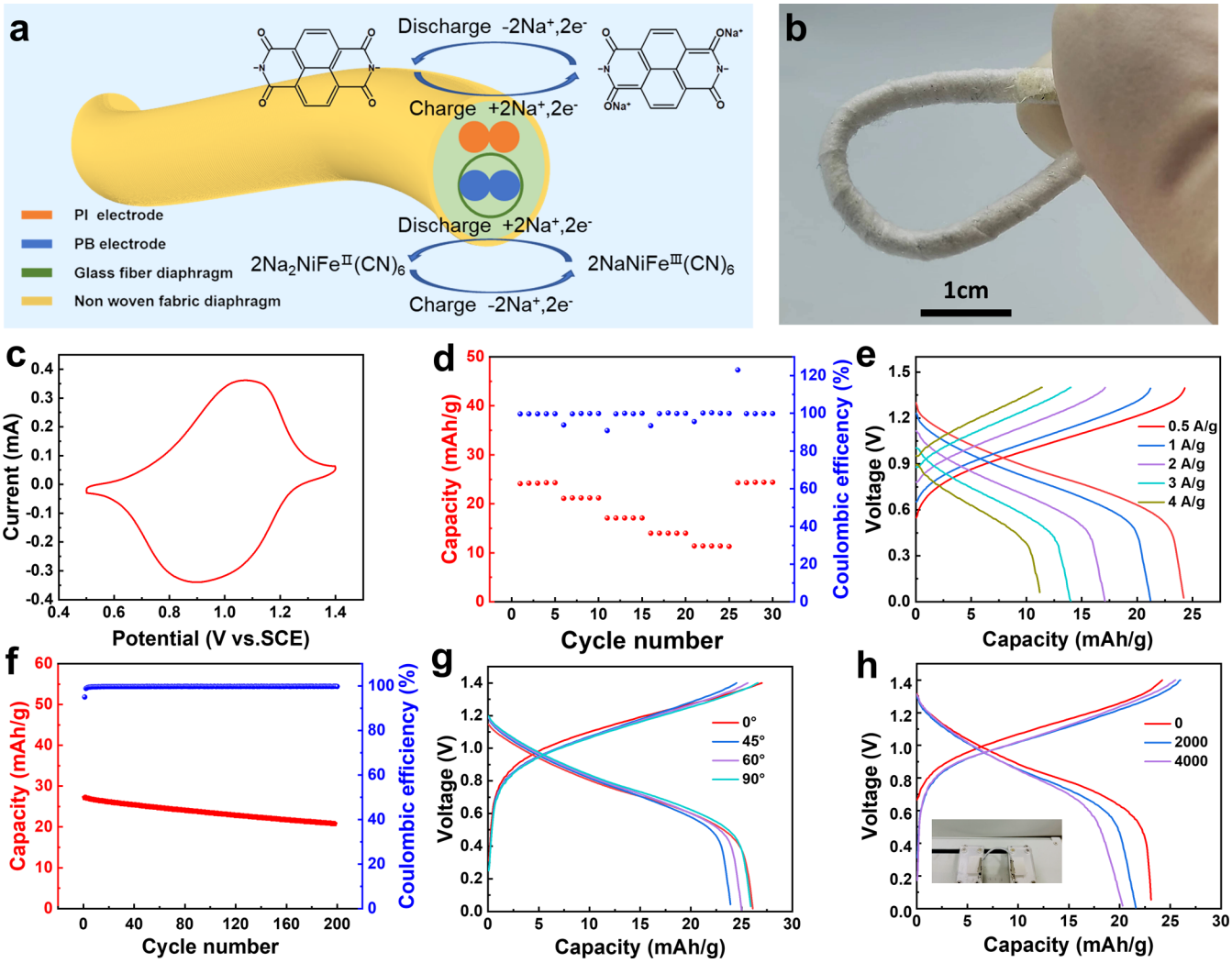

Figure 5. Performance of a yarn-shaped SWB (YSWB). (a) Schematic diagram of a YSWB manufactured with twisted yarn-shaped electrodes; (b) digital photo of a YSWB; (c) CV curve of a YSWB; (d) rate performance of a YSWB (current density from left to right is 0.5, 1.0, 2.0, 3.0, 4.0, and 0.5 A/g); (e) GCD curves of a YSWB at different current densities; (f) cyclic performance of a YSWB; (g) GCD curves of a YSWB at different bending angles; (h) durability testing of a YSWB.

compression force can be expressed with the following equation[34]

$$q = 2t\sin\frac{\theta}{2} \tag{1}$$

As the twist level increases, both the central angle θ and the stretching tension t gradually increase, ultimately leading to an increase in the compression force of the outer fiber toward the inner layer. Compared to the UYE, the adjacent fibers in the TYE are much closer. The active materials preloaded on the yarn electrode also change from a loose state to a dense state during the twisting process (Figure 3b). The twisting-induced structural change of the yarn from untwisting to twisting configurations could be verified with SEM. The SEM analysis reveals a substantial reduction in the overall dimensions of the TYE compared to the UYE, evident from both surface and cross-sectional views (Figure 3c). To quantify this phenomenon, the gap ratios of both electrodes were analyzed using ImageJ software based on the cross-sectional SEM images. Notably, the gap ratio of the UYE is ~30%, whereas that of the TYE is less than 12% (Figure 3d). Undoubtedly, this intimate contact between the active materials and carbon fibers in the TYE enhances its electrochemical performance in congruence with the findings presented in Figure 2f. However, it is crucial to recognize that an excessive increase in compression force may lead to the extrusion of active material slurry from internal spaces, potentially diminishing the specific capacitance of the TYE. This phenomenon could be observed in the yarn electrode prepared with the TAC technique at the twist level of 380 turns/m. Therefore, the twist should be controlled moderately in the TAC-based fabrication process to achieve the optimal performance.

The electrochemical performance of the UYE and TYE with the identical loading of Ni-HCF was measured to further verify the contribution of twisting. In comparison to the low specific capacity of 54.5 mAh/g obtained with UYE, a much higher reversible specific capacity of 64.2 mAh/g could be reached using TYE (Figure 4a). When the charge/discharge current density increases from 1.0 to 5.0 A/g, the specific capacity of the UYE reduces by 41.7%. In contrast, the specific capacity of the TYE decreases by only 21.5% (Figure 4b). The closer contact between the active material and fibers in the TYE may facilitate the quick transfer of ions and electrons, resulting in improved performance at greater charge/discharge current

https://doi.org/10.1021/acsami.4c16439
ACS Appl. Mater. Interfaces 2024, 16, 71038−71047

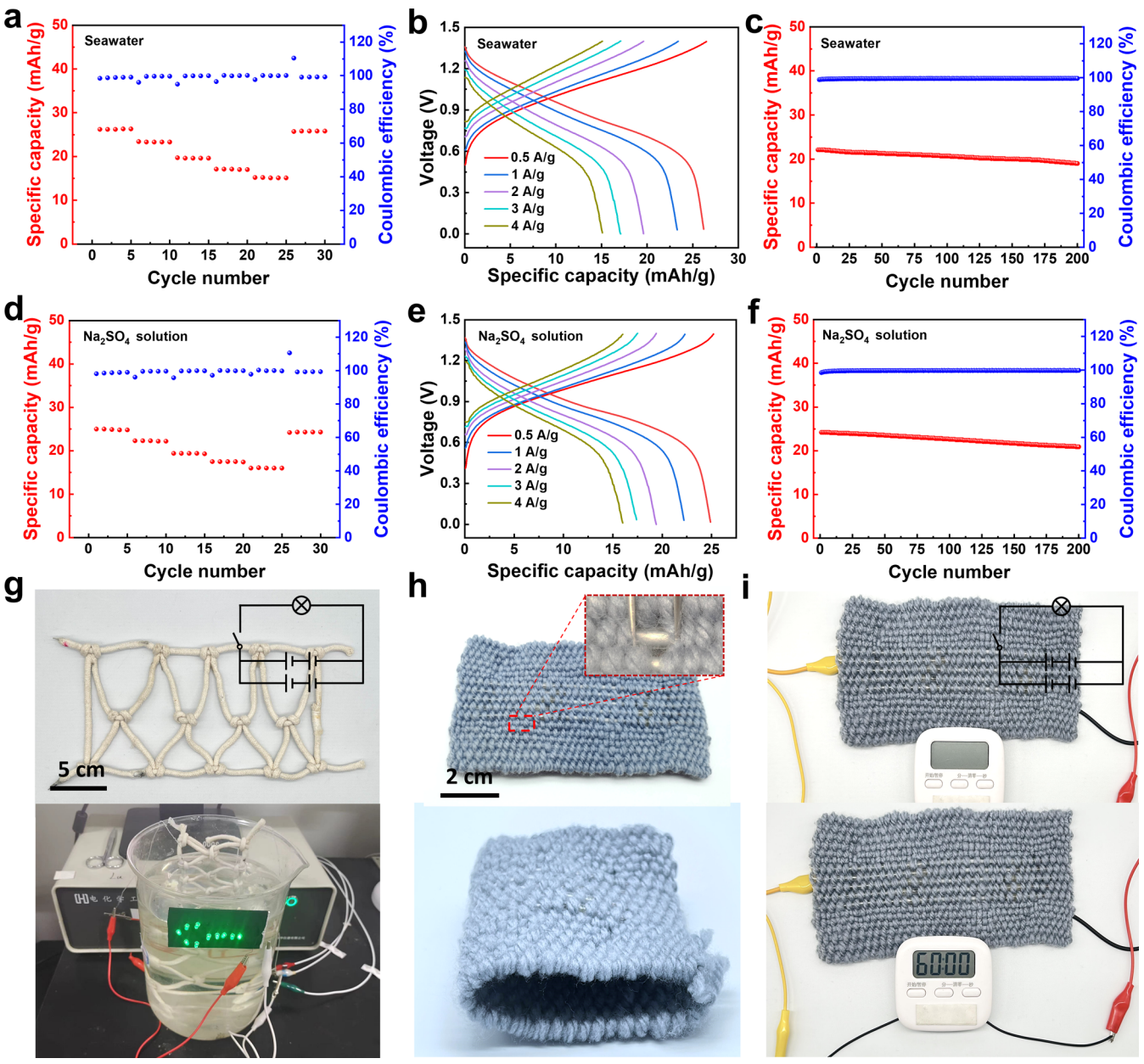

Figure 6. Feasibility of YSWBs. Rate performance (a), GCD curves (b), and cycling performance (c) of YSWBs in seawater; rate performance (d), GCD curves (e), and cycling performance (f) of YSWBs in 1.0 M Na_2SO_4 solution; (g) LEDs powered with a fishing net woven with YSWBs; (h) energy storage fabric woven with YSWBs; (i) a timer powered by the energy storage fabric for 1 h.

densities. The cycling performance of the electrodes was also tested at a current density of 1.0 A/g, showing that both have very similar retention rates after 200 cycles (Figure 4c).

To investigate the charging mechanism of Ni-HCF materials, the CV curves of the UYE and TYE were collected at scan rates ranging from 0.5 to 10 mV/s. In addition to the capacitive process, the surface redox reactions are also involved in the performance of the electrodes. Thus, the total current of the electrode can be described by the following equation[35]

$$i = av^b \tag{2}$$

where a and b are variable parameters, and v is the scanning rate. For the charging process controlled by the surface redox process, the current is proportional to the scanning rate, $b = 1$. However, for the diffusion-controlled charging process, the current is proportional to the square root of the scanning rate, $b = 0.5$. Formula (2) can be converted into the following equation

$$\log i = \log a + b \log v \tag{3}$$

Parameter b could be obtained from the CV curves measured at different scanning rates (Figure S3). It can be calculated from Figure 4d that b values for the UYE and TYE are 0.77 and 0.82, respectively, showing that the charge-storage mechanism of Ni-HCF follows both diffusion-controlled and capacitive-controlled processes.

During the ion intercalation/deintercalation, the diffusion process is slow and tends to be the control step. The diffusion coefficient is positively correlated with the reaction rate in this process. According to the Randles–Sevcik eq (25 °C)[36]

$$I_p = 26900n^{3/2}ACD^{1/2}v^{1/2} \tag{4}$$

https://doi.org/10.1021/acsami.4c16439
ACS Appl. Mater. Interfaces 2024, 16, 71038−71047

where n, A, C, D, and v represent the number of electrons transferred during the redox process, the working electrode area, the concentration of ions participating in the reaction, the diffusion coefficient, and the scanning rate, respectively. Since n, A, C, and v remain unchanged during the test, the diffusion coefficients can be compared qualitatively by comparing the slopes of the $I_p-v^{1/2}$ plots.[37] As shown in Figure 4e, the slope of the TYE is much higher than that of the UYE, indicating that the TYE possesses a higher sodium ion diffusion coefficient. PI, as a negative electrode active material, is capable of interacting with a range of monovalent and multivalent cations present in seawater.[38] In addition, PI has high capacity, excellent cycling performance, and good rate capability.[39,40] Thus, a PI-modified yarn was fabricated as the negative electrode to prepare a full battery (Figures S4−S6). The impedance spectra of the yarn-shaped SWBs were tested to analyze the charge transfer process (Figure 4f). The semicircle diameter of the curve for the TYE-based SWB is smaller than that for the UYE-based one, indicating the faster charge transfer in the TYE-based SWB. The above data further verify that twisting of the fibers could improve the electrochemical performance of the yarn-shaped electrode by accelerating the charge transfer process.

The Ni-HCF-modified and PI-modified yarn electrodes prepared using the TAC technique with a twist level of 330 turns/m were assembled to construct a yarn-shaped SWB (YSWB). The two electrodes were separated with a glass fiber diaphragm. A nonwoven fabric was used to encapsulate the SWBs for manufacturing a 5 cm-long battery due to its great hydrophilicity and excellent water permeability (Figure 5a,b). The CV curve of the YSWB shows a pair of redox peaks at 1.1 and 0.9 V (Figure 5c). Figure 5d,e exhibit the rate performance and the GCD curves at the current densities ranging from 0.5 to 4.0 A/g. The capacity of the YSWB was maintained at 76.1% of its original level after 200 charge/discharge cycles at a current density of 1.0 A/g (Figure 5f). Considering its potential applications in marine textiles, the flexibility of the YSWB should be evaluated in the present study. At bending angles of 0, 45, 60, and 90°, the battery exhibits relatively stable charge and discharge performance (Figure 5g). Moreover, after 4000 cycles of bending and release, its capacity only decreases by 12.1% (Figure 5h), which is sufficient to demonstrate the excellent tolerance of the YSWB to deformation.

The YSWB's performance in seawater was measured further to verify its potential in practical applications. As the charge and discharge current density increases from 0.5 to 4.0 A/g, the specific capacity of the device reduces from 26.2 to 15.2 mAh/g (Figure 6a,b). After 200 charge−discharge cycles, the retention rate of the specific capacity is 86% (Figure 6c). The performance of the YSWB in seawater is quite similar to that obtained in a 0.5 mol/L NaCl solution (Figure 5d−f), fulfilling the requirements of energy supply in deep sea. It is worth mentioning that the performance of the YSWBs in seawater is slightly better than that in 0.5 mol/L NaCl, which may be attributed to the intercalation/deintercalation of the cations other than Na^+, such as K^+ and Mg^{2+}, with PI.[38] The Na_2SO_4 solution has been widely used as an electrolyte in aqueous sodium-ion batteries.[41] The present study also examined the performance of the YSWB in 1.0 mol/L Na_2SO_4 solution. As shown in Figure 6d−f, the performance of the YSWB in the Na_2SO_4 solution is comparable to those in seawater and 0.5 mol/L NaCl solution. The YSWBs were woven into a fishing net-like textile to demonstrate their potential in practical applications. The textile was immersed in seawater to fully absorb the electrolyte. After charging, the fishing net can successfully power a light panel composed of 10 LEDs (Figure 6g), proving the potential of the YSWB as an energy source in seawater. It should be noted that the YSWB could also function as a weavable aqueous sodium-ion battery for textile electronics after encapsulation. Figure 6h shows an energy storage fabric woven with the Na_2SO_4 solution-soaked YSWBs encapsulated with thermoplastic tubes. The flexible energy storage fabric can be applied as a rechargeable energy source to power a timer for more than 60 min (Figure 6i), demonstrating the great potential of YSWBs for powering wearable devices. Four YSWBs were woven into the textiles at a series-parallel circuit, as illustrated in the inset of Figure 6g. Further experiments were conducted to investigate the impact of the YSWBs on *Chlorella vulgaris*, a species of green microalga. The findings indicate that the presence of the YSWBs does not markedly influence the growth of the microalga (Figure S7). Consequently, the SWBs may potentially be employed in marine environments without disrupting the ecosystem.

CONCLUSIONS

In summary, we have reported a TAC method, which involves modification of active materials on parallel aligned carbon fibers and moderate twisting of the fibers, for fabricating high-performance yarn-shaped electrodes. Using this technique, active materials could be distributed in the internal spaces and on the outermost surface of the carbon yarn, making full use of each carbon fiber. In addition, the twist level could affect the performance of the yarn electrode. The optimal twist level could facilitate the close contact between carbon fibers and active materials to reduce the charge transfer resistance, thus achieving an enhanced specific capacity. Under the same conditions, applying the TAC technique can increase the specific capacity of the yarn-shaped positive electrode by about 15.9%, reaching 64 mAh/g, compared with the conventional TBC technique. YSWBs were constructed using the Ni-HCF-modified and PI-modified electrodes prepared using the TAC method. The devices showed a specific capacity of 24.3 mAh/g, a capacity retention rate of 76.1% after 200 cycles, and tolerance to 4,000 times bending. The YSWBs could be woven into a fishing net-like textile to power a light panel composed of 10 LEDs. This work introduces a universal method for fabricating high-performance carbon yarn-based electrodes. It may inspire the development of weavable 1-D YSWBs for marine and deep-sea applications.

EXPERIMENTAL SECTION

Materials and Reagents. Ethylenediamine (EDA), *N*-methylpyrrolidone (NMP), and poly(vinylidene fluoride) (PVDF) were purchased from Aladdin Biochemical Technology Co., Ltd. (Shanghai, China). $Ni(NO_3)_2{\cdot}6H_2O$ was purchased from Adamas Reagent Co., Ltd. (Shanghai, China). Trisodium citrate was purchased from West Asia Chemical Co., Ltd. (Shandong, China). 1,4,5,8-Naphthalene tetracarboxylic dianhydride (NTCDA) and $Na_4[Fe(CN)_6]$ were bought from McLean Biochemical Technology Co., Ltd. (Shanghai, China). Carbon fiber yarns were purchased from Shanghai Qijie Carbon Company. Other chemicals were of analytical grade and directly used without purification. The seawater is collected from the Bohai Sea. The nonwoven fabric was commercially purchased from the local market in Chongqing, China.

Material Synthesis and Electrode Preparation. *Ni-HCF Preparation.* Three mmol $Ni(NO_3)_2{\cdot}6H_2O$ and 3.6 mmol trisodium

https://doi.org/10.1021/acsami.4c16439
ACS Appl. Mater. Interfaces 2024, 16, 71038−71047

citrate were dissolved in 50 mL of pure water to prepare solution A. Three mmol $Na_4[Fe(CN)_6]$ were dissolved in 50 mL of pure water to prepare solution B. The two solutions were mixed under vigorous stirring for 30 min to obtain a blue-green suspension. After stirring at 60 °C for another 15 h, the precipitate was collected via centrifugation at 7000 rpm for 15 min. After water-washing and vacuum-drying, the final products were harvested and stored at ambient conditions.

Preparation of PI. Twenty mmol NTCDA and 20 mmol EDA monomers were mixed in pure water, stirring at 80 °C for 2 h. The mixture was then transferred into a high-pressure autoclave, reacting at 200 °C for 12 h. The PI precipitate was collected via centrifugation at 7000 rpm for 10 min. After water-washing and vacuum-drying, the PI powder was obtained and stored at ambient conditions.

Preparation of Yarn-Based Electrode. The active material, conductive carbon black, and PVDF were mixed in a weight ratio of 8:1:1 to create a slurry containing an appropriate quantity of NMP as the solvent. In the case of the TBC method, the parallel carbon yarns were subjected to a twisting using a homemade apparatus at a specific speed, after which they were evenly coated with the slurry at a density of 0.225 mg/cm^2. In the TAC method, the slurry was initially scraped onto the parallel fibers and subsequently twisted to form a yarn-based electrode. The resulting yarn electrodes were then incubated in a vacuum oven at 80 °C for a period exceeding 12 h to thoroughly evaporate the solvent.

Fabrication of Yarn-Shaped Batteries. The yarn electrodes modified with Ni-HCF and PI were utilized as positive and negative electrodes, respectively, to produce yarn-shaped batteries. A positive electrode prewrapped with a 5 mm-wide diaphragm was aligned with a negative electrode in parallel. After covering it with a layer of nonwoven fabric, a yarn-shaped SWB was obtained. An aqueous sodium-ion battery containing the same electrodes was prepared with a Na_2SO_4 solution as the electrolyte and a thermoplastic tube as the encapsulating layer for performance comparison.

Characterization and Electrochemical Measurement. The morphologies of active materials and yarn electrodes were characterized using field-emission scanning electron microscopy (FESEM; JEOL, Tokyo, Japan). The crystal structure of Ni-HCF was measured using an X-ray diffractometer (XRD-7000 Shimadzu Corporation, Japan). Fourier transform infrared spectroscopy (FTIR, Nicolet 6700 Waltham, Massachusetts) was conducted to check the surface functional groups of PI. The hydrophilicity of yarn electrodes and carbon fibers was measured with a contact angle tester (model JC 2000D, Shanghai Zhongcheng Industrial Co., Ltd., China).

The electrochemical properties were measured with a three-electrode system consisting of a 1 cm-long yarn electrode (working electrode), a 1 cm^2 platinum plate (counter electrode), and a calomel electrode (reference electrode) in a 0.5 M NaCl solution. The CV curves and Nyquist plots were collected using a CHI 660E electrochemical workstation (Chenhua Instrument Co., Ltd.). The rate performance and cycling properties were tested using an automatic battery tester system (CT2001A, Wuhan LAND Electronics, China). Before each electrochemical test, N_2 gas was continuously introduced into the electrolyte for 40 min to purge O_2 efficiently. The repeated bending of the yarn-shaped battery was conducted on a flexibility tester (FT 2000, Prtronic, Shanghai Mifang Electronic Technology Co., Ltd., China) at a frequency of 0.5 Hz.

■ ASSOCIATED CONTENT

Supporting Information

The Supporting Information is available free of charge at https://pubs.acs.org/doi/10.1021/acsami.4c16439.

SEM image of a pretwisted carbon yarn (Figure S1); CV curves of a yarn-shaped Ni-HCF cathode in NaCl solution and seawater (Figure S2); CV curves of TYE and UYE at different scanning rates (Figure S3); characterization of PI and PI-modified electrode (Figure S4); CV curves of PI negative electrode in NaCl solution and seawater (Figure S5); electrochemical characterization of PI negative electrode and the full battery (Figure S6); growth curve of *Chlorella vulgaris* (Figure S7); and Comparison of performance between the YSWBs prepared in this work and reported SWBs (Table S1) (PDF)

■ AUTHOR INFORMATION

Corresponding Authors

Yan Qiao − *School of Materials and Energy, Southwest University, Chongqing 400715, P. R. China; Yibin Academy of Southwest University, Yibin 644000, P. R. China;* orcid.org/0000-0001-9701-4377; Phone: +86-23-68254732; Email: yanqiao@swu.edu.cn; Fax: +86-23-68254969

Zhisong Lu − *School of Materials and Energy, Southwest University, Chongqing 400715, P. R. China; Yibin Academy of Southwest University, Yibin 644000, P. R. China;* orcid.org/0000-0001-8879-4033; Email: zslu@swu.edu.cn

Authors

Yihao Jian − *School of Materials and Energy, Southwest University, Chongqing 400715, P. R. China; Yibin Academy of Southwest University, Yibin 644000, P. R. China*

Jun Ju − *School of Materials and Energy and College of Sericulture, Textile and Biomass Sciences, Southwest University, Chongqing 400715, P. R. China; Yibin Academy of Southwest University, Yibin 644000, P. R. China*

Lingwei Pei − *School of Materials and Energy, Southwest University, Chongqing 400715, P. R. China; Yibin Academy of Southwest University, Yibin 644000, P. R. China*

Wenhu Gao − *School of Materials and Energy, Southwest University, Chongqing 400715, P. R. China*

Duan Li − *School of Materials and Energy, Southwest University, Chongqing 400715, P. R. China*

Wei Wang − *Singapore Institute of Manufacturing Technology (SIMTech), Agency for Science, Technology and Research (A*STAR), Singapore 138634, Republic of Singapore*

Complete contact information is available at: https://pubs.acs.org/10.1021/acsami.4c16439

Notes

The authors declare no competing financial interest.

■ ACKNOWLEDGMENTS

This work was financially supported by the Chongqing Natural Science Foundation (Grant No. CSTB2023NSCQ-MSX0818), the Sichuan Science and Technology Program (Grant No. 2024YFHZ0192), the Innovation Research 2035 Pilot Plan of Southwest University (Grant No. SWU-XDPY22014), and the Science and Technology Innovation Program of General Administration of Sport of China (Grant No. 23KJCX042).

■ REFERENCES

(1) Hsu, S.-H.; Miao, J.; Zhang, L.; Gao, J.; Wang, H.; Tao, H.; Hung, S.-F.; Vasileff, A.; Qiao, S. Z.; Liu, B. An Earth-Abundant Catalyst-Based Seawater Photoelectrolysis System with 17.9% Solar-to-Hydrogen Efficiency. *Adv. Mater.* **2018**, *30* (18), No. 1707261.

(2) Hwang, S. M.; Park, J.-S.; Kim, Y.; Go, W.; Han, J.; Kim, Y.; Kim, Y. Rechargeable Seawater Batteries—From Concept to Applications. *Adv. Mater.* **2019**, *31* (20), No. 1804936.

(3) Jung, Y.; Lee, S.; Kim, D.; Lee, H.; Kim, S.; Cho, J.; Jin, H.; Kim, Y.; Park, J.-S.; Lee, W.-G. Vertically Arranged Electrode Structures

with High Energy Density for Seawater Batteries. *J. Power Sources* **2024**, *592*, No. 233960.
(4) Blake, I. C. Fiftieth Anniversary: The Anniversary Issue on Primary Cell: Silver Chloride-Magnesium Reserve Battery. *J. Electrochem. Soc.* **1952**, *99* (8), 202C.
(5) Coleman, J. R. Magnesium-lead Chloride Batteries. *J. Appl. Electrochem.* **1971**, *1* (1), 65−71.
(6) Prasad, K. V.; Venkatakrishnan, N.; Mathur, P. B. Preliminary Report on the Performance Characteristics of the Magnesium-mercurous Chloride Battery System. *J. Power Sources* **1976**, *1* (3), 371−375.
(7) Chen, J.; Sun, L.; Wang, K.; Zhang, Y. Research and Applications of Rechargeable Seawater Battery. *J. Energy Storage* **2024**, *76*, No. 109659.
(8) Kim, D. H.; Choi, H.; Hwang, D. Y.; Park, J.; Kim, K. S.; Ahn, S.; Kim, Y.; Kwak, S. K.; Yu, Y.-J.; Kang, S. J. Reliable Seawater Battery Anode: Controlled Sodium Nucleation Via Deactivation of the Current Collector Surface. *J. Mater. Chem. A* **2018**, *6* (40), 19672−19680.
(9) Kim, Y.; Kim, H.; Park, S.; Seo, I.; Kim, Y. Na ion- Conducting Ceramic as Solid Electrolyte for Rechargeable Seawater Batteries. *Electrochim. Acta* **2016**, *191*, 1−7.
(10) Li, M.; Dixit, M.; Essehli, R.; Jafta, C. J.; Amin, R.; Balasubramanian, M.; Belharouak, I. Na3Zr2Si2PO12 Solid Electrolyte Membrane for High-Performance Seawater Battery. *Adv. Sci.* **2023**, *10* (17), No. 2300920.
(11) Islam, M.; Jena, S.; Sidra, S.; Thanh Tran, D.; Hwan Kim, D.; Hoon Kim, N.; Hee Lee, J. Bifunctional Mo4O11 Nanosheets-Engineered Co-Ni Alloy Nanowires enable High-Efficiency Seawater Electrolysis and Zn-Seawater Battery. *Chem. Eng. J.* **2024**, *487*, No. 150664.
(12) Xu, Y.; Lv, H.; Lu, H.; Quan, Q.; Li, W.; Cui, X.; Liu, G.; Jiang, L. Mg/seawater Batteries driven Self-powered direct Seawater Electrolysis Systems for Hydrogen Production. *Nano Energy* **2022**, *98*, No. 107295.
(13) Xia, Q.; Li, Z.; Liu, D.; Song, N.; Zhang, N.; Ma, S.; Wu, Z.; Yuan, W. Highly Effective Electrolytes toward High-Performance Aluminum/Seawater Batteries. *Batteries Supercaps* **2024**, No. e202400307.
(14) Mulyadewi, A.; Mahbub, M. A. A.; Irmawati, Y.; Balqis, F.; Adios, C. G.; Sumboja, A. Rechargeable Zinc−Air Batteries with Seawater Electrolyte and Cranberry Bean Shell-Derived Carbon Electrocatalyst. *Energy Fuels* **2022**, *36* (10), 5475−5482.
(15) Popović, A. S.; Grgur, B. N. Carbon Felt-polypyrrole-silver Chloride Composite as a Rechargeable Positive Electrode for the Seawater Magnesium Cell. *Synth. Met.* **2023**, *295*, No. 117359.
(16) Le, Z.; Li, W.; Dang, Q.; Jing, C.; Zhang, W.; Chu, J.; Tang, L.; Hu, M. A high-power Seawater Battery Working in a Wide Temperature Range enabled by an Ultra-stable Prussian Blue Analogue Cathode. *J. Mater. Chem. A* **2021**, *9* (13), 8685−8691.
(17) Qiao, S.; Zhou, Q.; Ma, M.; Liu, H. K.; Dou, S. X.; Chong, S. Advanced Anode Materials for Rechargeable Sodium-Ion Batteries. *ACS Nano* **2023**, *17* (12), 11220−11252.
(18) Wen, W.; Geng, C.; Li, X.; Li, H.; Wu, J.-M.; Kobayashi, H.; Sun, T.; Zhang, Z.; Chao, D. A Membrane-Free Rechargeable Seawater Battery Unlocked by Lattice Engineering. *Adv. Mater.* **2024**, *36* (30), No. 2312343.
(19) Nimkar, A.; Gavriel, B.; Bergman, G.; Turgeman, M.; Fan, T.; Shpigel, N.; Aurbach, D. Rechargeable Seawater Batteries Based on Polyimide Anodes. *ACS Sustainable Chem. Eng.* **2023**, *11* (4), 1428−1433.
(20) Zhai, W.; Zhu, Z.; Sun, X.; Peng, H. Fiber Solar Cells from High Performances Towards Real Applications. *Adv. Fiber Mater.* **2022**, *4* (6), 1293−1303.
(21) Marriam, I.; Tebyetekerwa, M.; Chathuranga, H.; Sun, K.; Du, A.; Yan, C. Nickel-Rich Cathode Yarn for Wearable Lithium-Ion Batteries. *Adv. Fiber Mater.* **2024**, *6* (2), 341−353.
(22) Xu, Q.; Chen, J.; Loh, J. R.; Zhong, H.; Zhang, K.; Xue, J.; Lee, W. S. V. Fiber-Shaped Batteries Towards High Performance and Perspectives of Corresponding Integrated Battery Textiles. *Adv. Energy Mater.* **2024**, *14* (3), No. 2302536.
(23) Yang, Y.; Shao, Y.; Lu, G.; Shao, Y. Fusing Fibre Batteries Interface via Biomimetic Gel Electrolyte. *Adv. Fiber Mater.* **2024**, *6* (4), 949−951.
(24) Xiao, G.; Ju, J.; Lu, H.; Shi, X.; Wang, X.; Wang, W.; Xia, Q.; Zhou, G.; Sun, W.; Li, C. M.; Qiao, Y.; Lu, Z. A Weavable and Scalable Cotton-Yarn-Based Battery Activated by Human Sweat for Textile Electronics. *Adv. Sci.* **2022**, *9* (7), No. 2103822.
(25) Ju, J.; Xiao, G.; Jian, Y.; Wu, L.; Sun, W.; Wang, W.; Li, C. M.; Qiao, Y.; Lu, Z. Scalable, High-performance, Yarn-shaped Batteries Activated by an Ultralow Volume of Sweat for Self-powered Sensing Textiles. *Nano Energy* **2023**, *109*, No. 108304.
(26) Kim, Y.; Harzandi, A. M.; Lee, J.; Choi, Y.; Kim, Y. Design of Large-Scale Rectangular Cells for Rechargeable Seawater Batteries. *Adv. Sustainable Syst.* **2021**, *5* (1), No. 2000106.
(27) Kim, Y.; Shin, K.; Jung, Y.; Lee, W.-G.; Kim, Y. Development of Prismatic Cells for Rechargeable Seawater Batteries. *Adv. Sustainable Syst.* **2022**, *6* (6), No. 2100484.
(28) Lee, S.; An, G.-H. Interface Engineering of Carbon Fiber-Based Electrode for Wearable Energy Storage Devices. *Adv. Fiber Mater.* **2023**, *5* (5), 1749−1758.
(29) Chen, H.; Wang, J.; Guan, Z.; Tao, Y.; Li, L.; Wei, J.; Ma, S.; Yan, Z.; Han, J.; Wang, F.; Shen, Z.; Yang, D. Boosting the Overall Specific Capacity of SiO Electrodes for Lithium-ion Batteries using a Multifunctional Carbon Cloth Current Collector. *Mater. Chem. Front.* **2023**, *7* (20), 4993−5004.
(30) Zhang, X.; Li, J.; Ao, H.; Liu, D.; Shi, L.; Wang, C.; Zhu, Y.; Qian, Y. Appropriately Hydrophilic/hydrophobic Cathode enables High-performance Aqueous Zinc-ion Batteries. *Energy Storage Mater.* **2020**, *30*, 337−345.
(31) Wan, M.; Tang, Y.; Wang, L.; Xiang, X.; Li, X.; Chen, K.; Xue, L.; Zhang, W.; Huang, Y. Core-shell Hexacyanoferrate for Superior Na-ion Batteries. *J. Power Sources* **2016**, *329*, 290−296.
(32) Qian, J.; Wu, C.; Cao, Y.; Ma, Z.; Huang, Y.; Ai, X.; Yang, H. Prussian Blue Cathode Materials for Sodium-Ion Batteries and Other Ion Batteries. *Adv. Energy Mater.* **2018**, *8* (17), No. 1702619.
(33) Zhou, X.; Fang, S.; Leng, X.; Liu, Z.; Baughman, R. H. The Power of Fiber Twist. *Acc. Chem. Res.* **2021**, *54* (11), 2624−2636.
(34) Huang, W.; Fu, T.; Zhang, Y.; Wang, J. An Approach to Predict the Tensile Strength of a Two-ply Yarn from Single Filament Yarn. *J. Text. Inst.* **2017**, *108* (3), 412−417.
(35) Bhojane, P. Recent Advances and Fundamentals of Pseudocapacitors: Materials, Mechanism, and its Understanding. *J. Energy Storage* **2022**, *45*, No. 103654.
(36) Choi, C.; Ashby, D. S.; Butts, D. M.; DeBlock, R. H.; Wei, Q.; Lau, J.; Dunn, B. Achieving High Energy Density and High Power Density with Pseudocapacitive Materials. *Nat. Rev. Mater.* **2020**, *5* (1), 5−19.
(37) Elgrishi, N.; Rountree, K. J.; McCarthy, B. D.; Rountree, E. S.; Eisenhart, T. T.; Dempsey, J. L. A Practical Beginner's Guide to Cyclic Voltammetry. *J. Chem. Educ.* **2018**, *95* (2), 197−206.
(38) Nimkar, A.; Malchick, F.; Gavriel, B.; Turgeman, M.; Bergman, G.; Fan, T.; Bublil, S.; Cohen, R.; Weitman, M.; Shpigel, N.; Levi, M. D.; Aurbach, D. Influences of Cations' Solvation on Charge Storage Performance in Polyimide Anodes for Aqueous Multivalent Ion Batteries. *ACS Energy Lett.* **2021**, *6* (7), 2638−2644.
(39) Chen, L.; Bao, J. L.; Dong, X.; Truhlar, D. G.; Wang, Y.; Wang, C.; Xia, Y. Aqueous Mg-Ion Battery Based on Polyimide Anode and Prussian Blue Cathode. *ACS Energy Lett.* **2017**, *2* (5), 1115−1121.
(40) Zhang, M.; Wang, L.; Xu, H.; Song, Y.; He, X. Polyimides as Promising Materials for Lithium-Ion Batteries: A Review. *Nano-Micro Lett.* **2023**, *15* (1), 135.
(41) Ding, C.; Chen, Z.; Cao, C.; Liu, Y.; Gao, Y. Advances in Mn-Based Electrode Materials for Aqueous Sodium-Ion Batteries. *Nano-Micro Lett.* **2023**, *15* (1), 192.

https://doi.org/10.1021/acsami.4c16439
ACS Appl. Mater. Interfaces 2024, 16, 71038−71047